Applied Physics B (2022) 128:148
https://doi.org/10.1007/s00340-022-07868-x

Applied Physics B
Lasers and Optics

REGULAR PAPER

Extremely high birefringent slotted core umbrella-shaped photonic crystal fiber in terahertz regime

Sayed Asaduzzaman[1,3] · Hasin Rehana[1,3] · Touhid Bhuiyan[2] · Dhiman Sarma[1] · Osama S. Faragallah[4] · Mahmoud M. A. Eid[5] · Ahmed Nabih Zaki Rashed[6]

Received: 16 January 2022 / Accepted: 3 July 2022 / Published online: 19 July 2022

Abstract

In this research, we have suggested an umbrella-shaped cladding and slotted core photonic crystal fiber (PCF). The aimed PCF has been quantitatively inquired employing the full vectorial finite-element method (FV-FEM) at a broader span of frequency of 0.8–2.4 THz. The core region is arranged by rectangular slots and elliptical slots. Where rectangular slots are conformed to high-resistivity silicon (HRS) material and elliptical slots filled with epsilon near zero (ENZ) material. Cyclic olefin copolymer (TOPAS) was applied as the background material. PCF shows enormously eminent birefringence of 6.10×10^{-1}, low confinement loss of 3×10^{-9} dB/m, low effective material loss (EML) of 0.129 cm^{-1}, power fraction of 65.1% and scattering loss of 1.23×10^{-10} dB/km at a frequency of 1 THz. The effective area of 9.20×10^{-9} m^2, the nonlinearity of 9.56 W^{-1} km^{-1} and the V-parameter have also been investigated at 1 THz. A lower dispersion was achieved where the value of X-Axis is near zero and the value of Y-Axis is also near zero and flattened. The aimed PCF can be used for different optical communication systems under the terahertz regime.

1 Introduction

The frequency range of terahertz waves or radiation is 0.1–10 THz, which is between the microwave band and frequency span. Due to diverse applications of terahertz waveguides such as astronomy [1], imaging [2], communication [3], sensing [4], biomedical applications [5, 6], 6G Communication [7], milk purity [8], salinity [9] and temperature monitoring [10] researchers gives focus on terahertz-based devices. THz-based photonic crystal fiber has also been used nowadays for vast optical applications such as higher birefringence, lower confinement loss, high nonlinearity, and low dispersion properties [11, 12]. The organization of the architecture of photonic crystal fiber contains

✉ Ahmed Nabih Zaki Rashed
ahmed_733@yahoo.com

Sayed Asaduzzaman
asadcse.rmstu@gmail.com

Hasin Rehana
hasin.cse13@gmail.com

Touhid Bhuiyan
t.bhuiyan@daffodilvarsity.edu.bd

Dhiman Sarma
dhiman001@yahoo.com

Osama S. Faragallah
o.salah@tu.edu.sa

Mahmoud M. A. Eid
m.elfateh@tu.edu.sa

[1] Department of Computer Science and Engineering, Rangamati Science and Technology University, Rangamati, Bangladesh

[2] Department of Computer Science and Engineering, University of Dhaka, Dhaka, Bangladesh

[3] Department of Computer Science and Engineering, Daffodil International University, Dhaka, Bangladesh

[4] Department of Information Technology, College of Computers and Information Technology, Taif University, P.O. Box 11099, Taif 21944, Saudi Arabia

[5] Department of Electrical Engineering, College of Engineering, Taif University, P.O. Box 11099, Taif 21944, Saudi Arabia

[6] Electronics and Electrical Communications Engineering Department, Faculty of Electronic Engineering, Menoufia University, Menouf 32951, Egypt

tiny holes through the cylindrical cross-section of the fiber with background material. The holes are filled with air or liquids or different materials. Photonic crystal fiber (PCF) has design flexibility than the conventional fiber with better optical properties such as birefringence [13], nonlinearity [14], dispersion [15], confinement loss [16], sensitivity [17], biosensor applications [18], and terahertz applications [19].

PCF may be categorized into index guiding (IG) PCF and photonic bandgap (PBG) PCF. PCF with high birefringence and low confinement loss may be employed in a wide range of applications, including fiber lasers [20], fiber sensors [21], and gyroscopes [22]. Besides different novel structures of core and cladding, both core and cladding of PCF can be used for better optical properties. In [23], elliptical core and in [24], elliptical cladding has been used for higher birefringence. Rectangular holes have been used in [25] which shows higher birefringence of 10^{-3}.

A high birefringence of 2.1×10^{-2} and dispersion compensation octagonal PCF with a high negative dispersion of -562.52 ps/nm km at wavelength 1550 nm has been achieved [26]. A photonic crystal fiber with a hexagonal structure and rhombic air pits demonstrated impressive birefringence of 0.041 and nonlinearity of 4375 W^{-1} km^{-1} and 3960 W^{-1} km^{-1} for both the X-Axis and Y-Axis, respectively [27]. Honeycomb cladding and slotted hole core PCF were suggested by the authors in [28], which have better optical properties such as lower confinement loss of 10–8 cm^{-1}, a lower material loss of 0.095 cm^{-1}, and higher birefringence of 0.083. In [29], Sultana et al. suggested a PCF with near zero flattened dispersion of 0.53 ± 0.07 ps/THz/cm and ultra-high birefringence 0.086. The proposed PCF was organized with hexagonal cladding and elliptical hole-based slotted core where background material was used TOPAS.

In this paper, we proposed the optical characteristics of a new umbrella-shaped slot core photonic crystal fiber (US-PCF) and investigated them numerically. The proposed US-PCF simultaneously exhibits very high birefringence and very low inclusion loss. Besides, our suggested PCF also shows low dispersion properties as well as low scattering loss. Moreover, this photonic crystal fiber also shows potential results such as EML, effective area, nonlinearity and power fraction. The detailed structure has been described in the PCF architecture section and results have been illustrated in the results section. The results of the V-parameter of the suggested US-PCF show multimode properties from 0.9 to 2.4 THz frequency range. Our suggested US-PCF shows better results as well as various optical better properties in the terahertz regime compared to the previously suggested PCF.

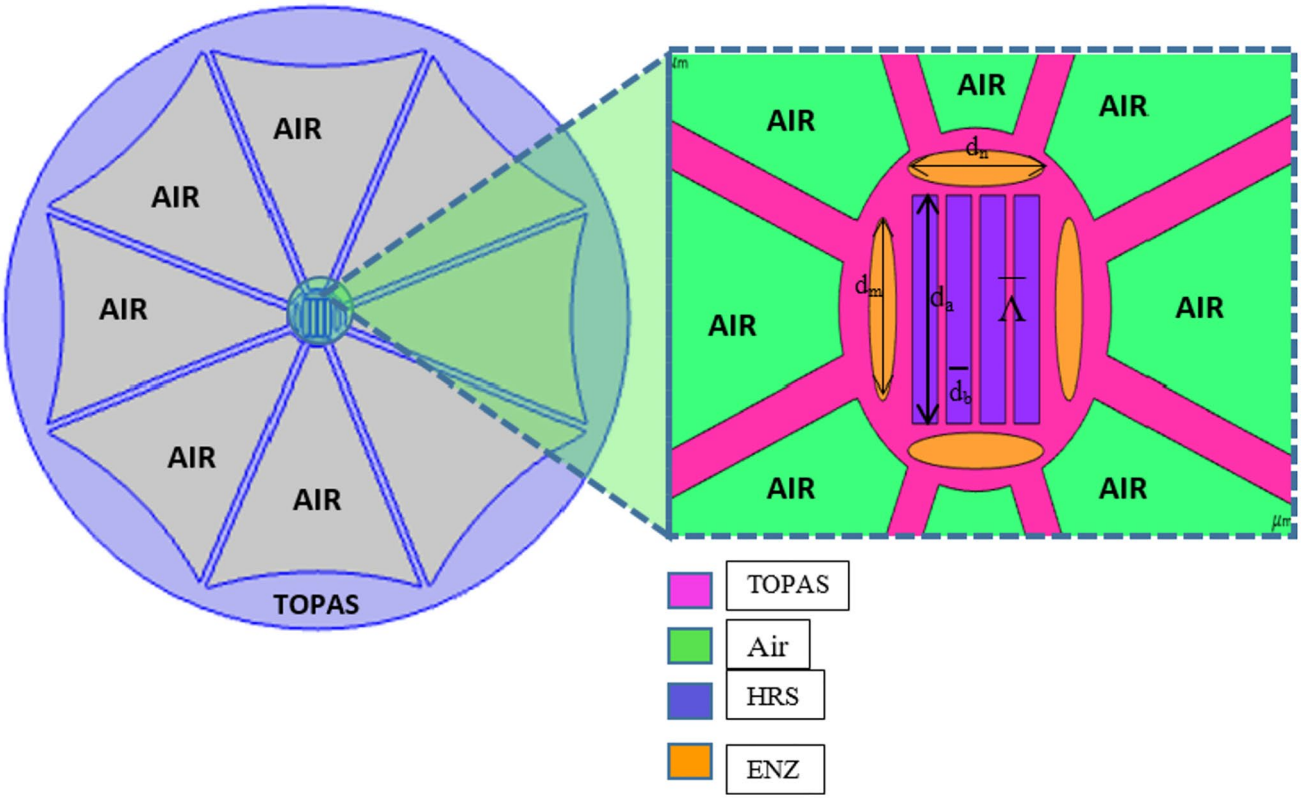

Fig. 1 Cross-sectional view and structure of the suggested UE-PCF

2 The proposed US-PCF architecture

Figure 1 shows a cross-section of the proposed umbrella-shaped slotted core PCF (US-PCF). The core region is shown in an enlarged view on the right side of the suggested structure. The suggested photonic crystal fiber is a hybrid structure with different core and clad arrangements. The cladding region is umbrella-shaped having eight sectors. The cladding region is filled with air. The core region is a slotted structure with both rectangular and elliptical holes. Four rectangular holes are arranged horizontally. The major axis is signified by $d_a = 100$ µm and the minor axis is referred to by $d_b = 15$ µm of the rectangular holes. The distance from the rectangular hole center to the center is denoted as the pitch and is indicated by $\Lambda = 30$ µm. Rectangular holes are filled with HRS whose refractive index is ($n_{\mathrm{HRS}} = 3.47$). Four elliptical holes are formatted in such a way that it is surrounded by the rectangular holes. The elliptical holes' major and minor axes are implied by $d_m = 40$ µm and $d_n = 8$ µm, respectively. Later in the results section, we used the term optimum. All the parameters given in this architecture section are the parameters of optimized structure PFUS-PCF. We have optimized these parameters and fixed the optimized structure of US-PCF by comparing it with porosity variation which has been shown in the results section. Epsilon near zero (ENZ) material with a refractive index of ($n_{\mathrm{ENZ}} = 0.1$) is used to fill elliptical holes. The proportion between the major and minor axis is named ellipticity. The ellipticity for rectangular and elliptical holes is signified by η_1 (d_a/d_b) and η_2 (d_m/d_n). The background material is TOPAS, with a refractive index of $n_{\mathrm{TOPAS}} = 1.53$. TOPAS has a stable refractive index over a wide wavelength range. A perfectly matched layer (PML) is kept at 10% of the overall fiber cross-section to meet the boundary constrain of the recommended PCF.

3 Numerical analysis

Numerical analysis of the suggested PCF has been inquired using FEM. Optical properties have been numerically looked into at a larger range of frequency from 0.8 to 2.4 THz in the terahertz regime. First, the difference between the major and minor axis is denoted as Birefringence B. In Eq. 1, n_x and n_y are called the effective mode index along with X-Polarization and Y-Polarization of the suggested PCF. In terahertz wave guidance, EML is an important property for photonic crystal fiber. Using Eq. 2, EML can be calculated for the suggested photonic crystal fiber [30]. In the equation, α_{mat} and E, are bulk material absorption loss and the electric field component, while ε_0, μ_0, and n are the permittivity in a vacuum, the permeability in vacuum, and the background material refractive index. Leakage or confinement loss is caused by light scattering through the cladding area. Equation 3 can be used to calculate the confinement loss [29] where f, c, and Im[neff] are the functioning frequency, the light speed, and the effective refractive index component. Equation 4 is used for the calculation of dispersion. Here, in the equation, c denotes the light velocity which is 3×10^8 m/s. n_{eff} denotes the mode effective refractive index for which the light passes through the core region.

$$B = \left| n_x - n_y \right|, \tag{1}$$

$$\mathrm{EML} = \frac{\sqrt{\frac{\varepsilon_0}{\mu_0}} \int\limits_{A_{\mathrm{mat}}} n\alpha_{\mathrm{mat}} |E|^2 dA}{2 \int\limits_{\mathrm{All}} S_Z dA}, \tag{2}$$

$$\mathrm{ConfinementLoss} = 8.686 \times \frac{(2\pi)f}{c} \mathrm{Im}(n_{\mathrm{eff}}), \tag{3}$$

$$\beta_2 = \frac{2}{3}\frac{dn_{\mathrm{eff}}}{d\omega} + \frac{\omega}{c}\frac{d^2 n_{\mathrm{eff}}}{d\omega^2}. \tag{4}$$

The entire quantity of power blowing over the suggested fiber is referred to power fraction which can be computed by Eq. 5. Here, integral of the region such as core, cladding, and holes has been taken by the numerator, whereas the integral of the whole fiber cross-section is taken by the denominator [31]. For the proposed US-PCF, the power fraction is defined as the ratio of the total power of the core, cladding and holes with total PCF power. Those powers are calculated by integration:

$$\mathrm{PowerFraction} = \frac{\int\limits_{X} S_z dA}{\int\limits_{\mathrm{All}} S_z dA}, \tag{5}$$

$$A_{\mathrm{eff}} = \frac{\left(\iint |E(x,y)^2| dxdy \right)^2}{\iint |E(x,y)|^4 dxdy}, \tag{6}$$

$$\gamma = \left(\frac{2\pi}{f} \right) \times \left(\frac{n_2}{A_{\mathrm{eff}}} \right) \left(\mathrm{W}^{-1}\mathrm{Km}^{-1} \right). \tag{7}$$

Equation 6 can be used to calculate the effective area A_{eff}, where E is considered the electric field. Equation 7 is used for calculating nonlinearity (γ). In Eq. 7, f is the operating frequency, the material's nonlinear coefficient is n_2, and A_{eff} is the effective area of the suggested fiber. Nonlinearity has a relation with the effective area, which is inversely proportional [32, 33]:

$$\alpha_R = C_R \times \left(\frac{f}{c}\right)^4 (\text{dB/Km}). \tag{8}$$

Scattering loss (α_R) can be computed by Eq. 8, where C_R is the scattering constant, f is the functioning frequency, and c is the light speed [34]. Numerical aperture can be computed by Eq. 9, where A_{eff} is the effective region and f is the controlling frequency [35]:

$$\text{NumericalAperture(NA)} = \sin\theta \approx \left[1 + \frac{\pi A_{\text{eff}}}{f^2}\right]^{-1/2}, \tag{9}$$

$$V = \frac{2\pi r f}{c}\sqrt{n_{\text{co}}^2 - n_{\text{cl}}^2}. \tag{10}$$

Equation 10 can be used to calculate the value of the V parametric quantity, where f, c, and r are the operating frequency, the light speed, and the core area radius of the suggested PCF while, n_{co} and ncl are the core refractive index and the cladding refractive index [33]. V parameter is used to measure the mode of the fiber whether it is multimode or single-mode. If the measurement of the v parameter is to a lesser extent of 2.405 then its mode is single mode. If the value is higher than 2.405 then it is called multimode fiber.

4 Results and discussion

To examine the optical attributes, FV-FEM along with perfectly matched layer (PML) is employed. The numerical investigation has been done using famous simulation software for optics COMSOL Metaphysics V5.5. Figure 2a and b illustrates the modal intensity of the suggested PCF at core territory. The convergence error of the suggested fiber is significantly depleted. The birefringence of the suggested umbrella-shaped slotted core PCF (US-PCF) and porosity variation of the fiber has been shown in Fig. 3. Porosity means the ellipticity of both rectangular slots and elliptical slots. In the investigation, we have decreased porosity by 10% and 15% where the optimized porosity was fixed. A decrease of porosity means the decrease of both the major axis and minor axis concurrently of both elliptical holes. But the decrease in porosity of elliptical holes makes holes more circular than elliptical ones. But these elliptical holes or increase of ellipticity makes higher birefringence. As we get higher Birefringence, we have fixed the optimum structure. From the figure, it is authorized that for optimized PCF we get higher birefringence. The birefringence curve alters with respect to the frequency. The Birefringence is increasing at a slow rate from 0.8 to 1.8 THz and then the birefringence curve is nearly flat from 1.8 to 2 THz, and after that the birefringence decreases up to 2.4 THz. We get the highest birefringence for optimized UC-PCF of 6.78×10^{-1} at 2 THz. The birefringence curve for different pitch values has been shown in Fig. 4. The birefringence curve changes as the frequency changes. The figure illustrates that the birefringence increases with respect to frequency up to 1.8 THz and decreases after the 2 THz at rate. Pitch is the distance between the center to the center of the rectangular slots. We have varied the pitch for optimized 5 µm, 10 µm and 15 µm to investigate the birefringence. Birefringence decreases largely at 15 µm whereas the birefringence is quite the same at 5 µm and 10 µm. Although from Fig. 4, it is clear that we get higher birefringence for 10 µm than 5 µm. We have optimized 5 µm for optimum PCF structure to keep the structure in proper organization and proper air filling proportion.

Effective material loss is a substantial attribute of the suggested UC-PCF structure. Figure 5 shows the effective material loss with respect to the different frequencies in terahertz where porosity also varied to fix the optimum structure. The EML curve shows that for optimum PCF we get higher EML than 15% porosity less but it is a bit high. Although the suggested PCF shows higher EML at optimum structure, for porosity 15% less the rule of air filling fraction will be broken and also causes fabrication problem of

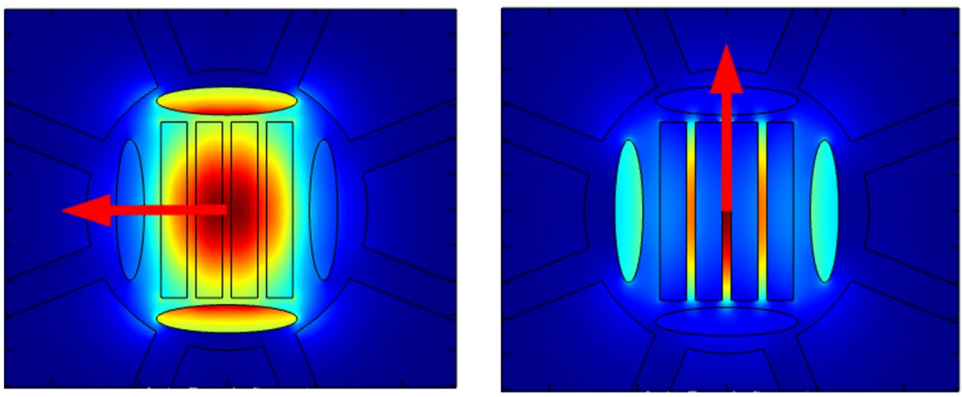

Fig. 2 The suggested PCF mode field distribution along **a** X-Axis and **b** Y-Axis at f = 1 THz

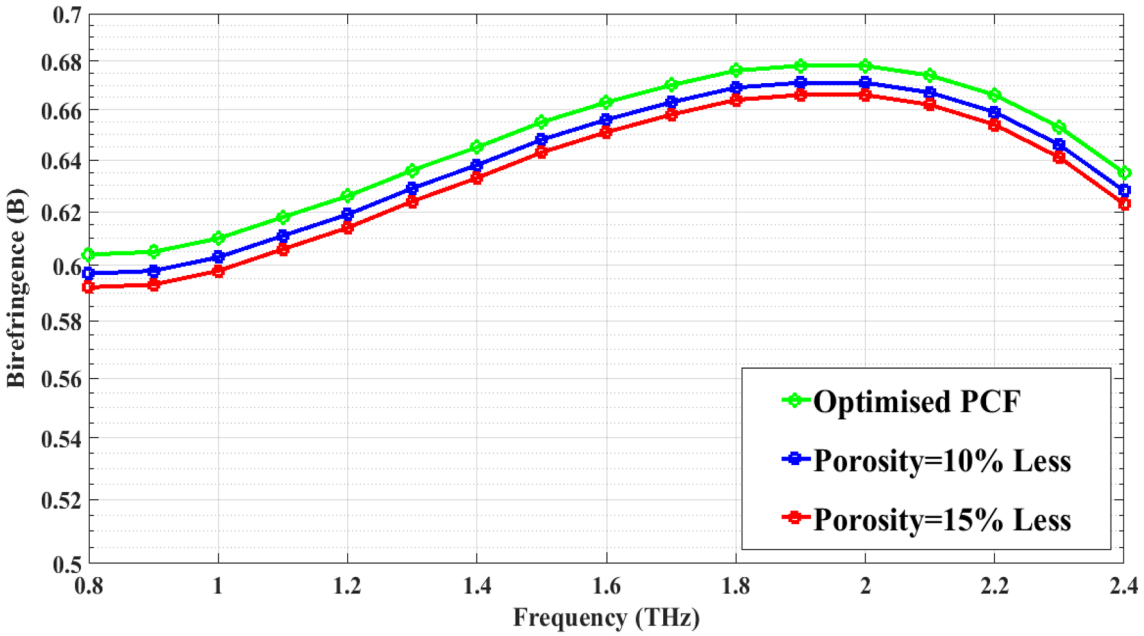

Fig. 3 Birefringence vs frequency for the suggested PCF according to porosity variation

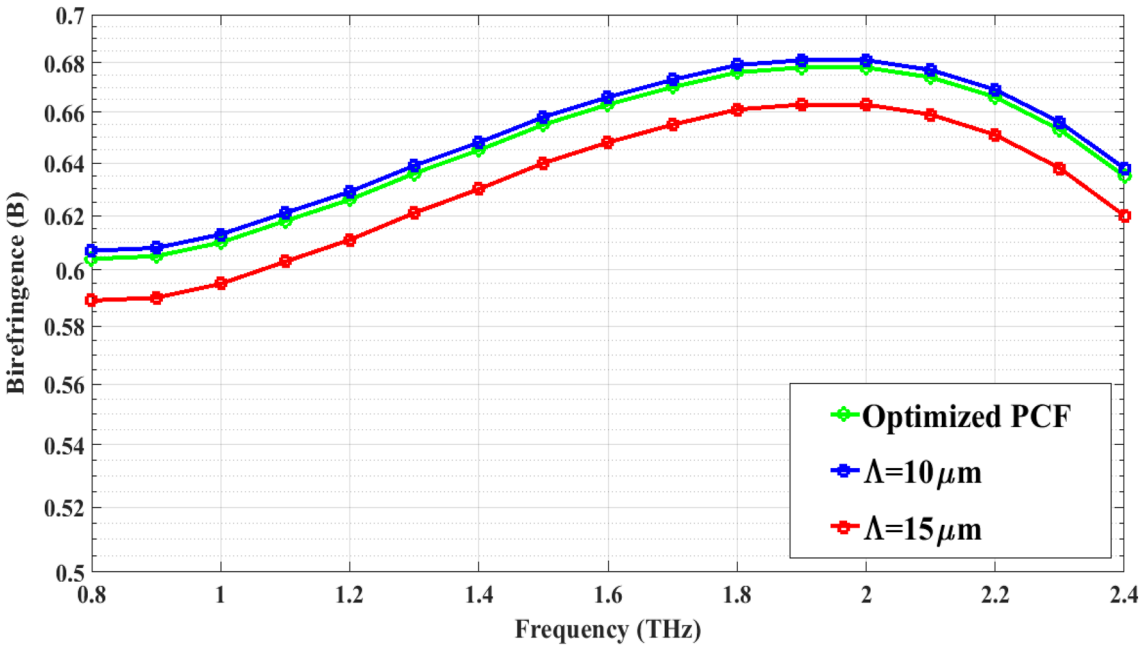

Fig. 4 Birefringence vs frequency for the suggested PCF according to pitch variation

the suggested fiber. Therefore, we have fixed optimum PCF. The EML curve gains at a fixed rate from 1 to 1.6 THz and then decrease from 1.7 to 2.4 THz which has been shown in Fig. 5. We get EML of 0.215 (cm^{-1}) for both 1.6 and 1.7 THz for optimum structure.

For the proposed umbrella-shaped cladding slotted core photonic crystal fiber (US-PCF), we acquire exceedingly lower confinement loss which has been shown in Fig. 6. The confinement loss curve we computed both for effective refractive index along X-Axis and Y-Axis. It can be illustrated that the confinement loss curve is almost flat for

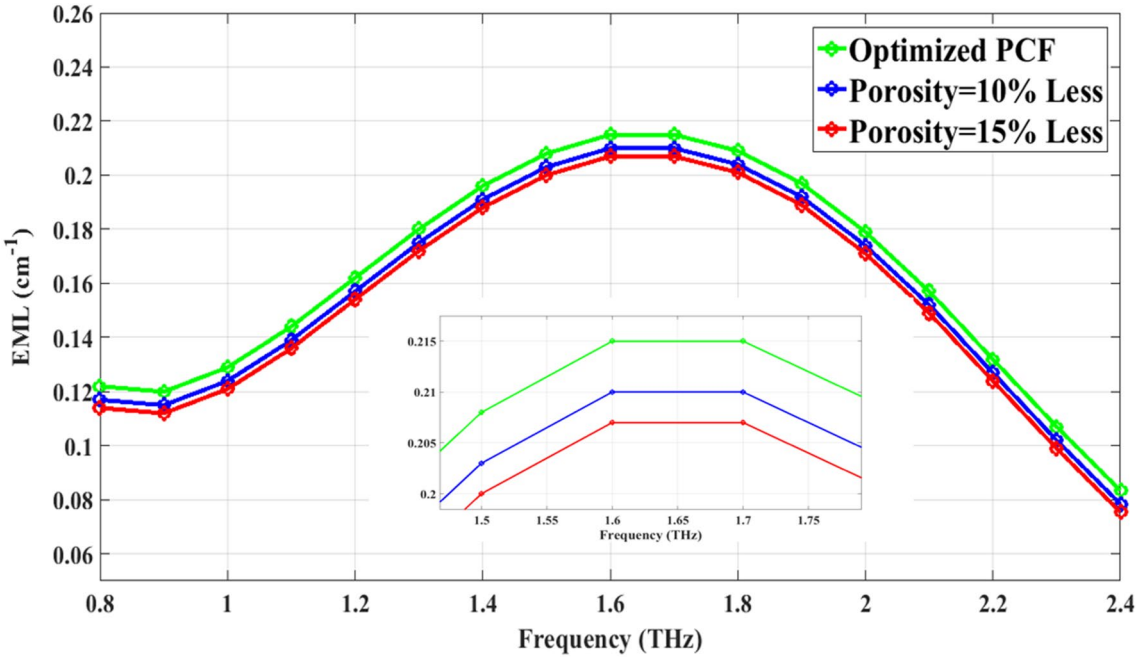

Fig. 5 Effective material loss vs frequency for the suggested PCF according to porosity variation

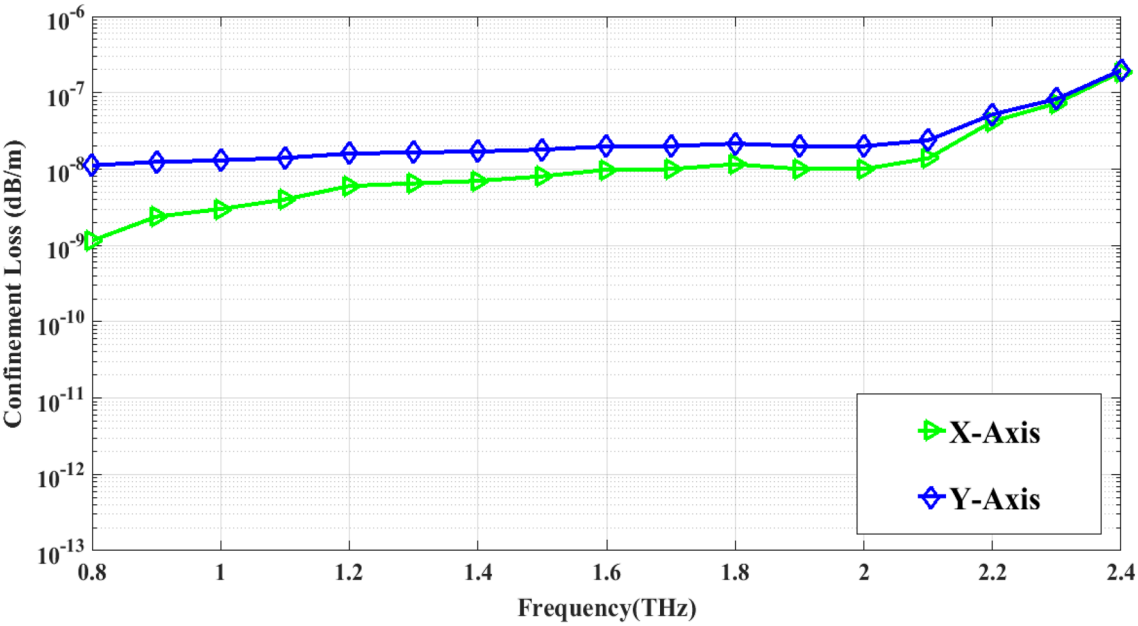

Fig. 6 Confinement loss vs frequency for the suggested PCF according to X-Axis and Y-Axis

both X-Axis and Y-Axis up to 2 THz. Then, both of the curves increase with respect to frequency. Lower confinement loss/leakage loss of 1.15×10^{-9} dB/m has been gained with X-Axis for 0.8 THz.

Figure 7 illustrates the dispersion curve for both X-Axis and Y-Axis. For the Y-axis, the dispersion is very low near zero and the curve is almost flat. For X-Axis, the dispersion also is very low but varies from 2 to − 1.25 ps/THz/cm.

Figure 8 shows the power fraction of the suggested US-PCF for both X-Axis and Y-Axis. The power fraction increases at a small rate from 0.8 to 2.4 THz.

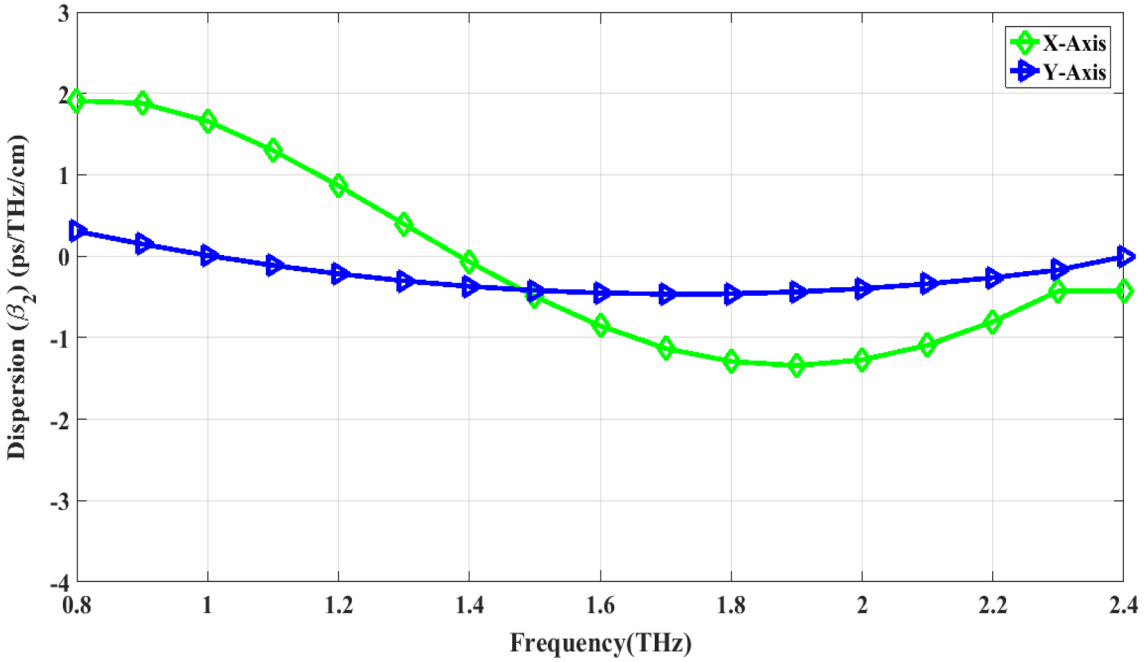

Fig. 7 Dispersion aperture vs frequency for the suggested PCF according to X-Axis and Y-Axis

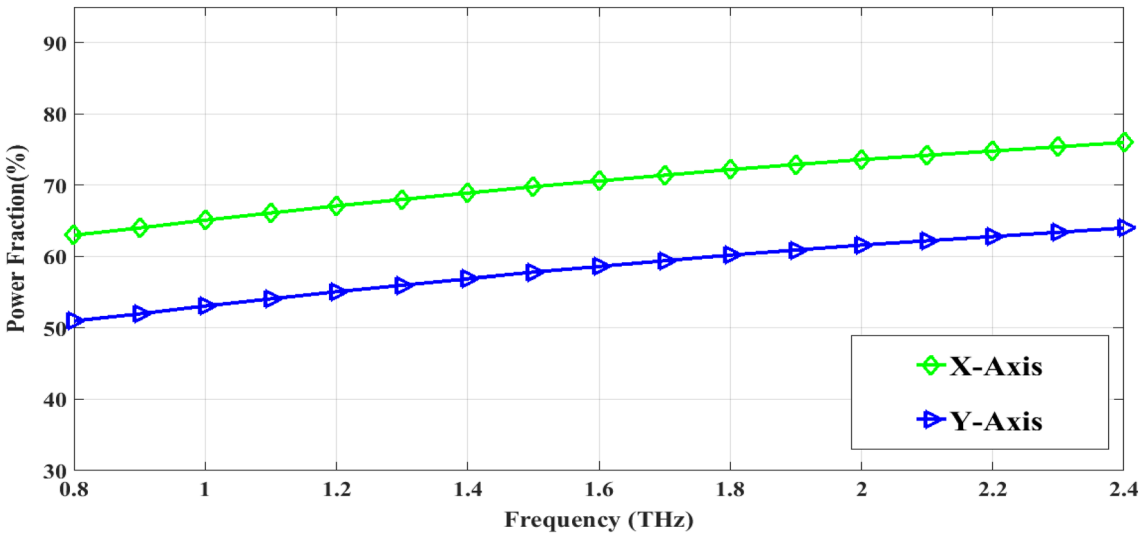

Fig. 8 Power fraction vs frequency for the suggested PCF according to X-Axis and Y-Axis

The effective area is demonstrated in Fig. 9 along the X-Axis and the Y-Axis. The effective area diminishes with the enhancement of frequency. For the X-Axis, we get frequencies the effective area of 9.70×10^{-9} m^2 and for the Y-Axis of 9.20×10^{-9} m^2 at frequency 0.8 THz. The relation between nonlinearity and effective area is reciprocally proportional (Fig. 10).

Figure 11 shows the numerical aperture of the suggested US-PCF for both X-Axis and Y-Axis. The quantity of light accepted or emitted is called numerical aperture (NA). The NA curve is slightly increasing at a flat rate according to the frequency. The higher value of NA is good for PCF as it means that the higher quantity of light accepts at the core area. The more light passes through the core region the lower the scattering loss which has been shown in Fig. 12. The scattering loss increases with the frequency from 0.8 to 2 THz. The lowest scattering loss has been gained at 0.8 THz, which is 5.05×10^{-11} dB/km.

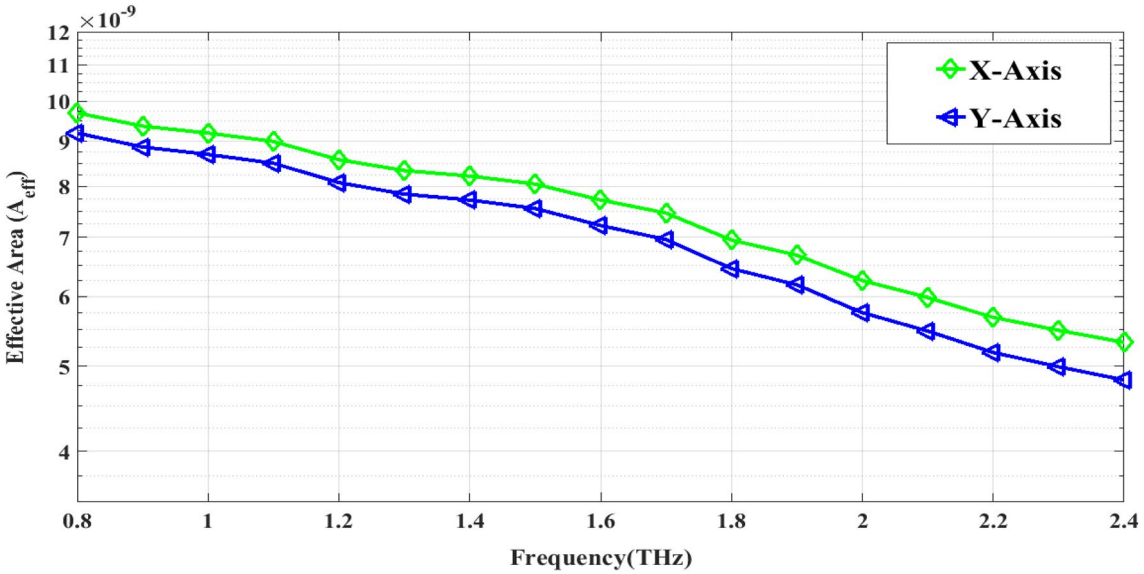

Fig. 9 Effective area vs frequency for proposed PCF according to X-Axis and Y-Axis

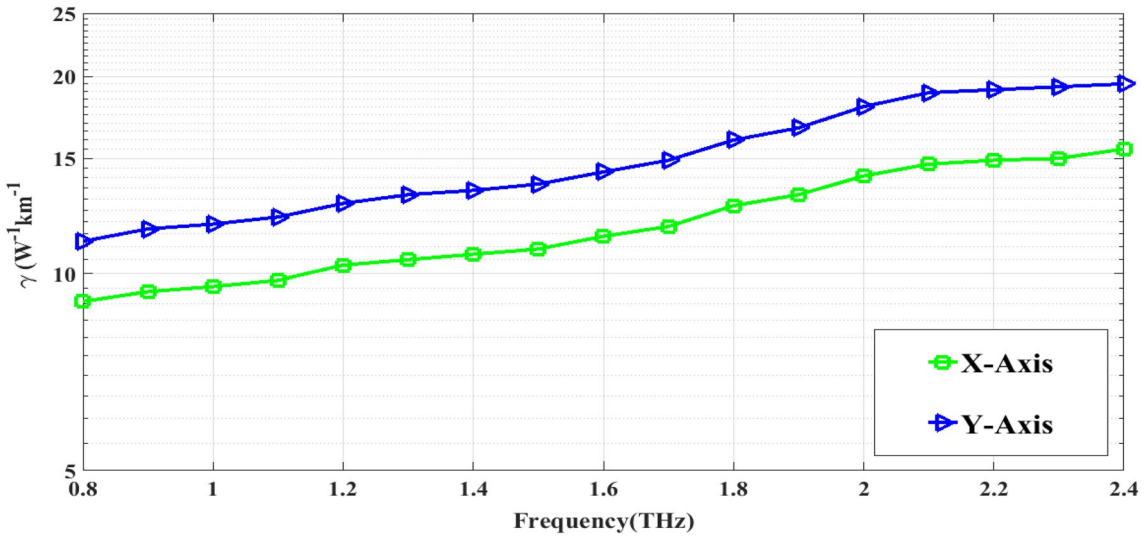

Fig. 10 Nonlinearity vs frequency for proposed PCF according to X-Axis and Y-Axis

V-parameter is an important optical property for proposed PCF. If the V-parametric quantity measurement is smaller than the value of 2.405 then the suggested PCF is single-mode and if the value is more than 2.405 then the proposed PCF is multimode. Figure 13 illustrates clearly that our suggested US-PCF shows single-mode properties at only a V-parameter value for 0.8 THz but at the frequency range from 0.9 to 2.4 THz, the suggested US-PCF is multimode.

A comparative study of the proposed PCF and anterior PCFs is demonstrated in Table 1. This table illustrates that the aimed PCF depicts better results for different optical properties. We have investigated more optical properties than the previous PCFs. Although some characteristics like EML other PCFs show better results but our suggested PCFs show very high birefringence as well as better EML, confinement loss, the fraction of power, NA, effective area, scattering loss, etc. at the same time for a wider frequency range.

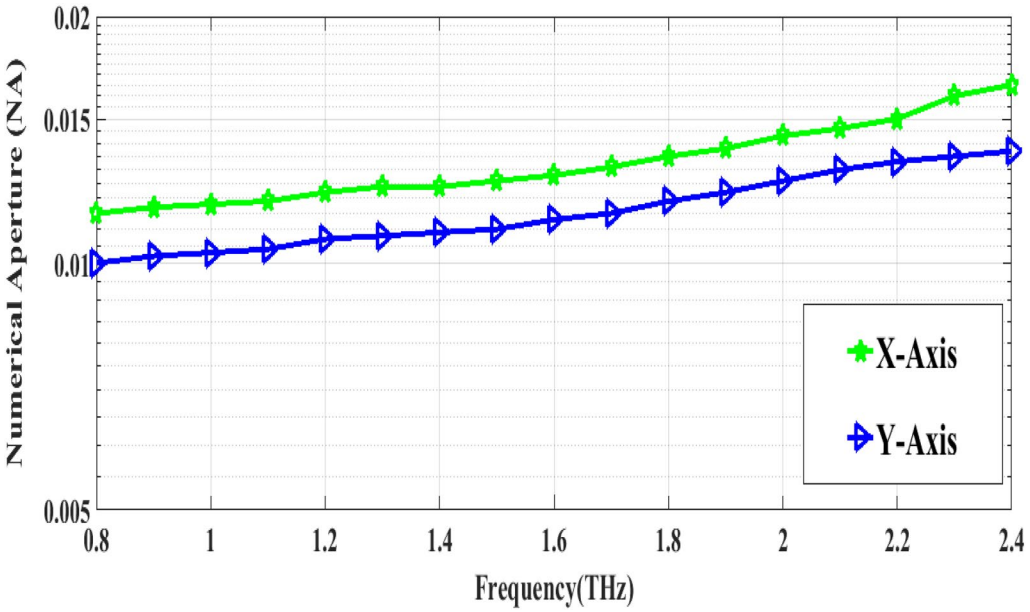

Fig. 11 Numerical aperture vs frequency for proposed PCF according to X-Axis and Y-Axis

Fig. 12 Scattering loss vs frequency for proposed PCF

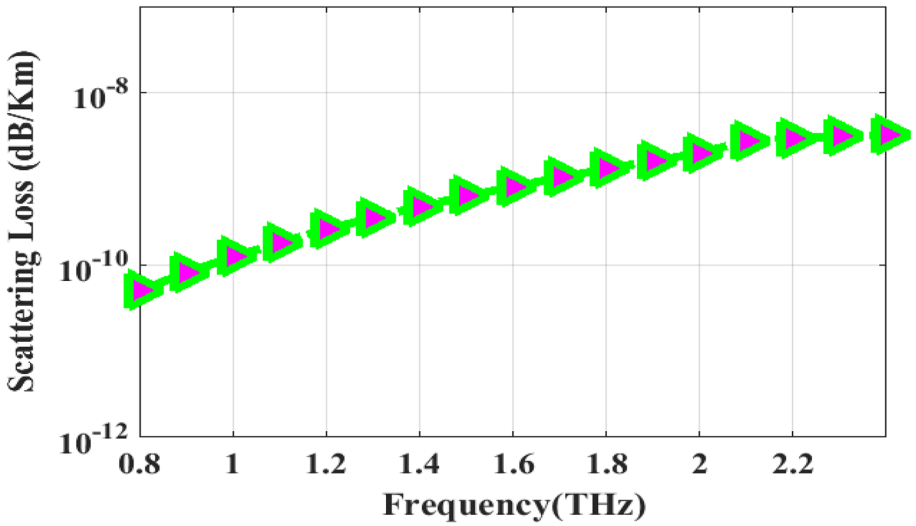

5 Fabrication issue

Fabrication of photonic crystal fibers is a critical issue for the proposed photonics system. In comparison to previously proposed PCFs, our proposed umbrella-shaped slotted core PCF is not as complicated [5, 7, 10, 12]. As the proposed PCF is a microstructure fiber, the main challenge is to design it. As a result, micrometer-scale fabrication is possible. One more problem is maintaining hole-to-hole distances in photonic crystal fiber in addition to creating holes. Drilling [41], die extraction [42], drawing and filling schemes [43], chemical vapor deposition scheme [44], and stacking [45] are examples of recent advanced fabrication technology that can easily facilitate the proposed PCF fabrication. Furthermore, in the new era of 3-D printing technology, scientists have been drawn to it for the fabrication of microstructures such as optical fibers or photonic crystal fibers [45].

In the research [46], a single polarization single-mode (SPSM) PCF has been proposed. The structure of this PCF is formed with an array of air holes in a hexagonal formation. So for fabrication, a lot number of holes are needed to be made at cladding. Besides in the core region, there are rectangular slots of different shapes. Moreover, the operating frequency of this research is 1.10–1.74 THz. Another

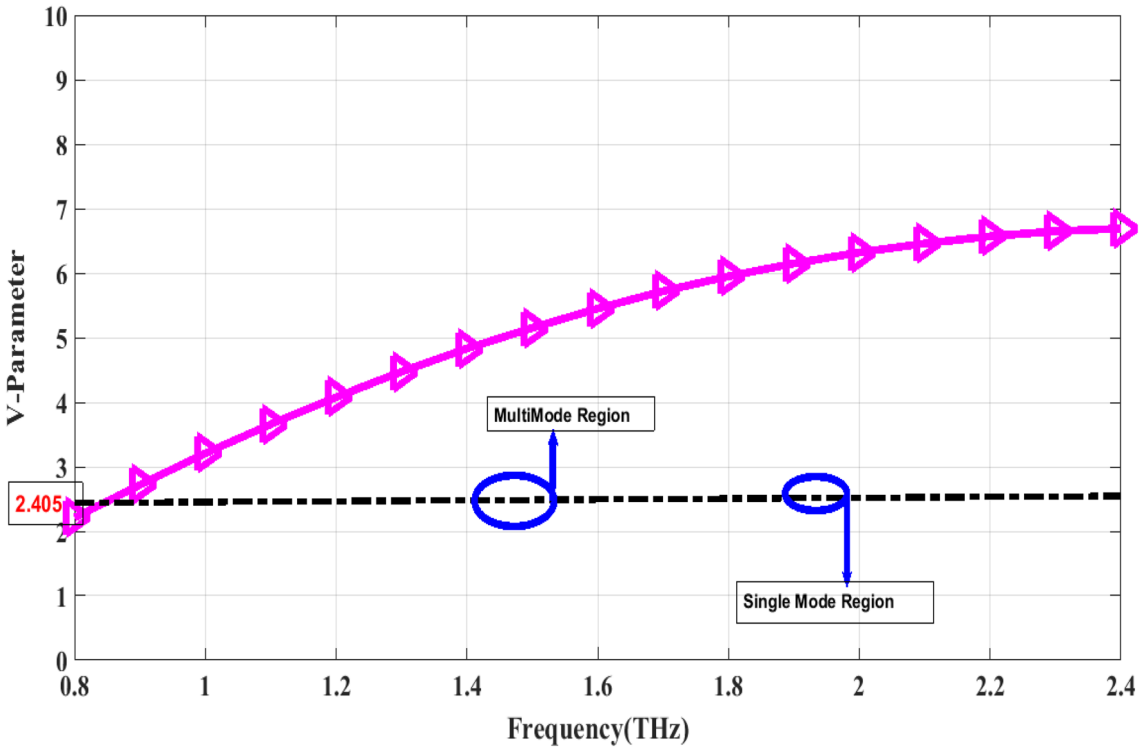

Fig. 13 V-parameter vs frequency for proposed PCF

Table 1 Comparability of the suggested PCF and prior PCFs at $f = 1$ THz

	Birefringence	EML	Conf loss	Power fraction (%)	NA	Effective area	Scattering loss
Suggested PCF	6.10×10^{-1}	0.129	3×10^{-9}	65.1	1.18×10^{-2}	9.20×10^{-9}	1.23×10^{-10}
[36]	–	0.076	8.96×10^{-1}	53	–	9.77×10^{-8}	–
[37]	–	0.038	2.35×10^{-1}	56	–	6.75×10^{-5}	9.64×10^{-10}
[38]	–	0.07	1.14×10^{-3}	–	–	1.07×10^{-9}	–
[39]	–	0.089	1×10^{-2}	37	–	9.77×10^{-8}	–
[40]	3×10^{-2}	0.098	5×10^{-11}	–	–	–	–

single-polarization SPSM has also been proposed in [47]. In this PCF, the cladding region is formed with lots of circular holes in a hexagonal formation with circular holes at the core. The operating wavelength is 0.9–1.4 THz. Fabrication of PCF with lots of holes is challenging, whereas our US-PCF contains only umbrella sectored holes at the cladding and similar types (elliptical and rectangular) holes at the core. Besides our operating wavelength is 0.8–2.4 THz. Moreover, long-distance communication systems, special laser systems such as fiber gyroscopes and polarization-sensitive optical modulators, and optical fiber sensing can all benefit from high birefringence [48, 49].

6 Conclusion

A slotted core (rectangle and elliptical slots) and umbrella-shaped cladding founded PCF has been suggested and numerically inquired at a broader range of frequency from 0.8 to 2.4 THz. The aimed PCF demonstrates extremely high birefringence as well as very low confinement loss than the previous suggested PCF. Besides low EML, high effective area, high power fraction, numerical aperture, nonlinearity, and scattering loss have also been investigated which also shows better results. Dispersion properties have also been investigated as our suggested PCF also shows near zero and flattened dispersion of ± 0.15 ps/THz for the Y-Axis and close zero dispersion of 0.7 ± 1.2 ps/THz for X-Axis.

TOPAS was used as background material whereas at the core both HRS and ENZ materials have been used for the suggested PCF. The intended PCF shows better results and many optical properties than the prior PCFs.

Acknowledgements This study was funded by the Deanship of Scientific Research, Taif University Researchers Supporting Project number (TURSP-2020/08), Taif University, Taif, Saudi Arabia.

Declarations

Conflict of interest The authors announce no conflicts of interest.

References

1. M.S. Islam, J. Sultana, S. Rana, M.R. Islam, M. Faisal, S.F. Kaijage, D. Abbott, Extremely low material loss and dispersion flattened TOPAS based circular porous fiber for long distance terahertz wave transmission. Opt. Fiber Technol. **34**, 6–11 (2017)
2. R.M. Woodward, V.P. Wallace, D.D. Arnone, E.H. Linfield, M. Pepper, Terahertz pulsed imaging of skin cancer in the time and frequency domain. J. Biol. Phys. **29**(2), 257–259 (2003)
3. T. Nagatsuma, G. Ducournau, C.C. Renaud, Advances in terahertz communications accelerated by photonics. Nat Photonics. **10**, 371–379 (2016). https://doi.org/10.1038/nphoton.2016.65
4. M.S. Islam, J. Sultana, K. Ahmed, M.R. Islam, A. Dinovitser, B.W.H. Ng, D. Abbott, A novel approach for spectroscopic chemical identification using photonic crystal fiber in the terahertz regime. IEEE Sens. J. **18**(2), 575–582 (2017)
5. K.I. Zaytsev, K.G. Kudrin, V.E. Karasik, I.V. Reshetov, S.O. Yurchenko, In vivo terahertz spectroscopy of pigmentary skin nevi: pilot study of non-invasive early diagnosis of dysplasia. Appl. Phys. Lett. **106**(5), 053702 (2015)
6. C.B. Reid, A. Fitzgerald, G. Reese, R. Goldin, P. Tekkis, P.S. O'Kelly et al., Terahertz pulsed imaging of freshly excised human colonic tissues. Phys. Med. Biol. **56**(14), 4333 (2011)
7. W. Xu, P. Guo, X. Li, Z. Hui, Y. Wang, Z. Shi, Y. Shu, Sheet-structured bismuthene for near-infrared dual-wavelength harmonic mode-locking. Nanotechnology **31**(22), 225209 (2020)
8. U. Biswas, J.K. Rakshit, G.K. Bharti, Design of photonic crystal microring resonator based all-optical refractive-index sensor for analyzing different milk constituents. Opt. Quant. Electron. **52**(1), 1–15 (2020)
9. S. Akter, K. Ahmed, S.A. El-Naggar, S.A. Taya, T.K. Nguyen, V. Dhasarathan, Highly sensitive refractive index sensor for temperature and salinity measurement of seawater. Optik **216**, 164901 (2020)
10. I.S. Amiri, B.K. Paul, K. Ahmed, A.H. Aly, R. Zakaria, P. Yupapin, D. Vigneswaran, Tri-core photonic crystal fiber based refractive index dual sensor for salinity and temperature detection. Microw. Opt. Technol. Lett. **61**(3), 847–852 (2019)
11. Z. Shen, K. Li, C. Jia, H. Jia, Mid-infrared dual-cladding photonic crystal fiber with high birefringence and high nonlinearity. Opt. Rev. **27**(3), 296–303 (2020)
12. Y. Zhang, X. Jing, D. Qiao, L. Xue, Rectangular porous-core photonic-crystal fiber with ultra-low flattened dispersion and high birefringence for terahertz transmission. Front. Phys. **8**, 370 (2020)
13. L. An, Z. Zheng, Z. Li, T. Zhou, J. Cheng, Ultrahigh birefringent photonic crystal fiber with ultralow confinement loss using four airholes in the core. J. Lightwave Technol. **27**(15), 3175–3180 (2009)
14. X. Li, Z. Xu, W. Ling, P. Liu, Design of highly nonlinear photonic crystal fibers with flattened chromatic dispersion. Appl. Opt. **53**(29), 6682–6687 (2014)
15. S.A. Razzak, Y. Namihira, Tailoring dispersion and confinement losses of photonic crystal fibers using hybrid cladding. J. Lightwave Technol. **26**(13), 1909–1914 (2008)
16. S. Asaduzzaman, K. Ahmed, T. Bhuiyan, T. Farah, Hybrid photonic crystal fiber in chemical sensing. Springerplus **5**(1), 1–11 (2016)
17. M.S. Islam, B.K. Paul, K. Ahmed, S. Asaduzzaman, M.I. Islam, S. Chowdhury et al., Liquid-infiltrated photonic crystal fiber for sensing purpose: design and analysis. Alex. Eng. J. **57**(3), 1459–1466 (2018)
18. S. Asaduzzaman, K. Ahmed, Investigation of ultra-low loss surface plasmon resonance-based PCF for biosensing application. Results Phys. **11**, 358–361 (2018)
19. K. Ahmed, M. Islam, S. Sen, B.K. Paul, S. Chowdhury, M. Hasan et al., Low-loss single mode terahertz microstructure fiber with near-zero-flattened dispersion. Adv. Sci. Eng. Med. **9**(10), 829–836 (2017)
20. Y. Zhao, F. Xia, J. Li, Sensitivity-enhanced photonic crystal fiber refractive index sensor with two waist-broadened tapers. J. Lightwave Technol. **34**(4), 1373–1379 (2016)
21. X. Wang, N. Song, J. Song, W. Li, A photonic crystal fiber with optimized birefringence-stress stability for fiber optic gyroscope. Optik **206**, 163488 (2020)
22. L. Sojka, P. Jaworski, W. Gora, D. Furniss, A. Seddon, P. Mergo et al., Polarization-maintaining erbium doped photonic crystal fiber laser. Laser Phys. **22**(1), 240–247 (2012)
23. F. Li, M. He, X. Zhang, M. Chang, Z. Wu, Z. Liu, H. Chen, Elliptical As2Se3 filled core ultra-high-nonlinearity and polarization-maintaining photonic crystal fiber with double hexagonal lattice cladding. Opt. Mater. **79**, 137–146 (2018)
24. P. Szarniak, R. Buczynski, D. Pysz, I. Kujawa, M. Franczyk, R. Stepien, Highly birefringent photonic crystal fibers with elliptical holes. In *Photonic Crystals and Fibers* (Vol. 5950, p. 59501L). International Society for Optics and Photonics (2005)
25. G. Jiang, Y. Fu, Y. Huang, High birefringence rectangular-hole photonic crystal fiber. Opt. Fiber Technol. **26**, 163–171 (2015)
26. M.I. Hasan, S.A. Razzak, M.S. Habib, Design and characterization of highly birefringent residual dispersion compensating photonic crystal fiber. J. Lightwave Technol. **32**(23), 3976–3982 (2014)
27. Z. Hui, Y. Zhang, A.H. Soliman, Mid-infrared dual-rhombic air hole $Ge_{20}Sb_{15}Se_{65}$ chalcogenide photonic crystal fiber with high birefringence and high nonlinearity. Ceram. Int. **44**(9), 10383–10392 (2018)
28. M.R. Islam, M.F. Kabir, K.M.A. Talha, M.S. Arefin, Highly birefringent honeycomb cladding terahertz fiber for polarization-maintaining applications. Opt. Eng. **59**(1), 016113 (2020)
29. J. Sultana, M.S. Islam, M. Faisal, M.R. Islam, B.W.H. Ng, H. Ebendorff-Heidepriem, D. Abbott, Highly birefringent elliptical core photonic crystal fiber for terahertz application. Opt. Commun. **407**, 92–96 (2018)
30. M.R. Hasan, M.S. Anower, M.A. Islam, S.M.A. Razzak, Polarization-maintaining low-loss porous-core spiral photonic crystal fiber for terahertz wave guidance. Appl. Opt. **55**(15), 4145–4152 (2016)
31. S. Rana, A.S. Rakin, M.R. Hasan, M.S. Reza, R. Leonhardt, D. Abbott, H. Subbaraman, Low loss and flat dispersion Kagome photonic crystal fiber in the terahertz regime. Opt. Commun. **410**, 452–456 (2018)
32. S. Coen, A.H.L. Chau, R. Leonhardt, J.D. Harvey, J.C. Knight, W.J. Wadsworth, P.S.J. Russell, White-light supercontinuum generation with 60-ps pump pulses in a photonic crystal fiber. Opt. Lett. **26**(17), 1356–1358 (2001)

33. S. Asaduzzaman, K. Ahmed, Proposal of a gas sensor with high sensitivity, birefringence and nonlinearity for air pollution monitoring. Sens. Bio-Sens. Res. **10**, 20–26 (2016)
34. Y. Wang and G. Jiang, Design and research of ultra-low loss terahertz photonic crystal fiber. In *4th Optics Young Scientist Summit (OYSS 2020)* (Vol. 11781, p. 117811A). International Society for Optics and Photonics (2021)
35. F.A. Mou, M.M. Rahman, M.A. Al Mahmud, M.R. Islam, & M.I.H. Bhuiyan, Design and characterization of a low loss polarization maintaining photonic crystal fiber for THz regime. In *2019 IEEE International Conference on Telecommunications and Photonics (ICTP)* (pp. 1–4). IEEE (2019)
36. M.R. Hasan, M.A. Islam, A.A. Rifat, A single mode porous-core square lattice photonic crystal fiber for THz wave propagation. J. Eur. Opt. Soc.-Rapid Public. **12**(1), 1–8 (2016)
37. B.K. Paul, K. Ahmed, Analysis of terahertz waveguide properties of Q-PCF based on FEM scheme. Opt. Mater. **100**, 109634 (2020)
38. J. Sultana, M.S. Islam, K. Ahmed, A. Dinovitser, B.W.H. Ng, D. Abbott, Terahertz detection of alcohol using a photonic crystal fiber sensor. Appl. Opt. **57**(10), 2426–2433 (2018)
39. M.R. Hasan, M.A. Islam, M.S. Anower, S.M.A. Razzak, Low-loss and bend-insensitive terahertz fiber using a rhombic-shaped core. Appl. Opt. **55**(30), 8441–8447 (2016)
40. T. Yang, C. Ding, R.W. Ziolkowski, Y.J. Guo, Circular hole ENZ photonic crystal fibers exhibit high birefringence. Opt. Express **26**(13), 17264–17278 (2018)
41. K. Nielsen, H.K. Rasmussen, A.J.L. Adam, P.C.M. Planken, O. Bang, P.U. Jepsen, Bendable, low-loss Topas fibers for the terahertz frequency range. Opt. Express **17**(10), 8592–8601 (2009)
42. S. Atakaramians, V.S. Afshar, H. Ebendorff-Heidepriem, M. Nagel, B.M. Fischer, D. Abbott, T.M. Monro, THz porous fibers: design, fabrication and experimental characterization. Opt. Express **17**(16), 14053–15062 (2009)
43. H.W. Lee, M.A. Schmidt, R.F. Russell, N.Y. Joly, H.K. Tyagi, P. Uebel, P.S.J. Russell, Pressure-assisted melt-filling and optical characterization of Au nano-wires in microstructured fibers. Opt. Express **19**(13), 12180–12189 (2011)
44. A. Amezcua-Correa, J. Yang, C.E. Finlayson, A.C. Peacock, J.R. Hayes, P.J.A. Sazio, J.J. Baumberg, S.M. Howdle, Surface-enhanced Raman scattering using microstructured optical fiber substrates. Adv. Funct. Mater. **17**(13), 2024–2030 (2007)
45. P.S.J. Russell, Photonic-crystal fibers. J. Lightw. Technol. **24**(12), 4729–4749 (2006)
46. T. Yang, C. Ding, R.W. Ziolkowski et al., An epsilon-near-zero (ENZ) based, ultra-wide bandwidth terahertz single-polarization single-mode photonic crystal fiber. J. Lightwave Technol. **39**(1), 223–232 (2021)
47. T. Yang, C. Ding, R.W. Ziolkowski et al., A Terahertz (THz) single-polarization-single-mode(SPSM) photonic crystal fiber (PCF). Materials **12**(15), 2442 (2019)
48. T.A. Birks, J.C. Knight, P.S.J. Russell, Endlessly single-mode photonic crystal fiber. Opt. Lett. **22**(13), 961–963 (1997)
49. K. Saitoh, M. Koshiba, Single-polarization single-mode photonic crystal fibers. IEEE Photon. Technol. Lett. **15**(10), 1384–1386 (2003)